

# NJC

Accepted Manuscript



This is an *Accepted Manuscript*, which has been through the Royal Society of Chemistry peer review process and has been accepted for publication.

*Accepted Manuscripts* are published online shortly after acceptance, before technical editing, formatting and proof reading. Using this free service, authors can make their results available to the community, in citable form, before we publish the edited article. We will replace this *Accepted Manuscript* with the edited and formatted *Advance Article* as soon as it is available.

You can find more information about *Accepted Manuscripts* in the [Information for Authors](#).

Please note that technical editing may introduce minor changes to the text and/or graphics, which may alter content. The journal's standard [Terms & Conditions](#) and the [Ethical guidelines](#) still apply. In no event shall the Royal Society of Chemistry be held responsible for any errors or omissions in this *Accepted Manuscript* or any consequences arising from the use of any information it contains.



[www.rsc.org/njc](http://www.rsc.org/njc)

Theoretical investigations on one- and two-photon absorptions  
for a series of covalently functionalized hybrid materials based  
on graphene

Li Zhang,<sup>1</sup> Lu-Yi Zou,<sup>1</sup> Jing-Fu Guo,<sup>2</sup> Ai-Min Ren\*,<sup>1</sup> Dan Wang,<sup>1</sup> Ji-Kang Feng<sup>1</sup>

<sup>1</sup>State Key Laboratory of Theoretical and Computational Chemistry,

Institute of Theoretical Chemistry, Jilin University,

Changchun 130061, People's Republic of China

<sup>2</sup>School of Physics, Northeast Normal University, 130024, P. R. China

\*Corresponding author: Tel./fax: +86-431-88498567 (A. M. Ren)

E-mail addresses: aimin\_ren@yahoo.com

**Abstract:** The covalently linked porphyrin-graphene composite materials with excellent nonlinear optical (NLO) properties and solubility have been experimentally studied recently, but the two-photon absorption (TPA) properties of them have not been reported yet. In this work, a series of novel graphene-like molecules and the corresponding hybrids with porphyrin have been designed to study on their one-photon absorption (OPA) and TPA properties as well as the structure-property relationships by employing quantum-chemical calculation. The maximum TPA cross sections ( $\delta_{max}$ ) calculated by means of the ZINDO method, combining with the FTRNLO-JLU program compiled by our group, are as large as  $\sim 913.0 - 3904.3$  GM. Moreover, both molecular size and porphyrin result in a significant increase of the  $\delta_{max}$  values. Furthermore, the hybrid molecules possess higher TPA response resulting from the intramolecular charge transfer, comparing with their counterpart without a porphyrin. The calculated results support the experimentally observed trends, as well as indicate that the designed compounds with large TPA cross sections are potential for applications involving optical limiting and two-photon fluorescence microscopy (TPFM). We expect that this study will provide a theoretical perspective for designing novel TPA materials based on graphene for further applications in the future.

**Keywords:** Graphene; Porphyrin; Hybrids; Two-photon Absorption

## 1. Introduction

In recent years, two-photon absorption (TPA) has increasingly become one of the most important research fields. The development of new organic compounds with efficient TPA properties and highly fluorescent quantum yields ( $\Phi$ ) is a subject with broad scientific and technological interest for a variety of applications including three-dimensional (3D) fluorescence microscopy,<sup>1</sup> optical limiting,<sup>2</sup> photodynamic therapy,<sup>3</sup> frequency up-converted lasing,<sup>4</sup> and two-photon fluorescent labeling.<sup>5</sup> In this regard, designing and developing novel practical TPA materials possessing enormous potentialities are thought to be the most important thing to meet the urgent need for the rapid development of various applications.

Graphene has attracted extensive attention in recent years because of its striking mechanical, optical, and electrical features. It was discovered in 2004,<sup>6</sup> and it is the most optimal planar nanometer material with a one-atom-thick crystal of carbon. With the thickness of just 0.35 nm, it is the thinnest planar nanometer material in the world. The structural simplicity is responsible for its possession of many excellent electronic and mechanical properties,<sup>7-10</sup> which gives it have a significant application prospect in optoelectronics and information, as well as new energy materials,<sup>11-16</sup> such as resonators,<sup>9</sup> organic photovoltaic devices,<sup>13</sup> sensitizers in solar cells,<sup>14</sup> catalysts,<sup>16</sup> and so on.

However, the poor solubility and processability of graphene makes it the primary issue for many perspective applications of graphene-based materials. So far, in order to improve its forming processing property and solubility to take better advantage of its excellent properties, the covalent functionalization of visible-light electron donors to graphene has been used as a method to compose novel graphene materials, by introducing special functional groups to overcome the obstacles of low solubility and rather poor processability in many kinds of solvents,<sup>17-21</sup> which can expand its applications. Recently, the studies on porphyrin-graphene hybrid materials have been reported by Chen and co-workers, revealing that covalent combinations can be a better approach to improve nonlinear optical (NLO) properties of graphene,<sup>22</sup> because both graphene and porphyrin possess large  $\pi$ -electron conjugation which are ideal to fulfill the requirement of a perfect NLO material. Therefore, the porphyrin-graphene hybrid materials enhancing the optical nonlinearities through large delocalized  $\pi$ -electron systems are considered to be novel NLO materials of choice in the future.<sup>23</sup>

To our knowledge, the TPA properties of porphyrin-graphene hybrid materials have remained unclear until now. Herein, to estimate the TPA characteristics of porphyrin-graphene hybrids, the aim of the present study is to construct novel molecules based on graphene and well-defined functionalized hybrid molecules with porphyrin and make investigations

towards the description of the influence of the size and the introduction of porphyrin, as well as the intramolecular charge transfer on their one- and two-photon absorptions by theoretical calculations. In addition, another goal of this work is to obtain good TPA materials with high two-photon absorption cross sections ( $\delta_{max}$ ), which can be applied in many fields, such as two-photon fluorescence microscopy (TPFM), optical limiting and so on. We hope our theoretical investigations will provide a new insight into the design of novel molecules based on graphene and corresponding hybrid molecules.

## 2. Theoretical methods

All of the calculations were performed with the Gaussian 09 program package<sup>24</sup> in this work. In this context, the DFT (Density Functional Density) method with the Coulomb-attenuated version of the Becke three-parameter hybrid B3LYP functional, CAM-B3LYP<sup>25</sup> exchange-correlation and 6-31G\* basis set was used to optimize the ground-state geometries of all investigated molecules. This functional allows for tuning proportion of exact Hartree-Fock exchange, and it is also able to improve the determination of various properties and describe transitions which involves different intermediate states with both valence and charge transfer features, crucially charge transfer excitation energy, without an obvious increase in computational cost compared to B3LYP.<sup>26,27</sup>

On the basis of optimized structures, the one-photon absorption spectra were also systematically investigated by time-dependent DFT (TD-DFT) at the same level, that is TD-DFT//CAM-B3LYP/6-31G\*.

To better understand the OPA and TPA properties of the studied molecules, the single and double electronic excitation configuration interactions (SDCI) were also employed by the Zerner's intermediate neglect of differential overlap (ZINDO) program.<sup>28</sup> Differing from one-photon absorption, the two-photon absorption process corresponds to the simultaneous absorption of two photons. The TPA efficiency at optical frequency  $\omega/2\pi$  of an organic molecule can be characterized by the TPA cross section  $\delta(\omega)$ , which are directly related to the imaginary part of the third-order polarizability  $\gamma(-\omega; \omega, -\omega, \omega)$  by<sup>29,30</sup>

$$\delta(\omega) = \frac{3\hbar\omega^2}{2n^2c^2\varepsilon_0} L^4 \text{Im}[\gamma(-\omega; \omega, -\omega, \omega)] \quad (1)$$

In which  $\gamma(-\omega; \omega, -\omega, \omega)$  refers to the third-order polarizability,  $\hbar\omega$  is the energy of incoming photons,  $n$  is on behalf of the refractive index of medium,  $c$  stands for the speed of light,  $\varepsilon_0$  denotes the vacuum electric permittivity, and  $L$  corresponds to the local-field factor. In the present calculations,  $n$  and  $L$  are set to 1 because of an isolated molecule in vacuum.

The sum-over-states (SOS) expression to evaluate the second hyperpolarizability  $\gamma_{ijkl}$  ( $i, j, k$ , and  $l$  refer to the molecular axis) can be deduced, using perturbation theory by considering a Taylor expansion of

energy with respect to the applied fields. The Cartesian components  $\gamma_{ijkl}$  are given by refs 31 and 32.

To compare the calculated  $\delta$  value with the experimental data, the damping factor ( $\Gamma_K$ ) of excited state  $K$  in the SOS expression is set to 0.14 eV,<sup>33,34,35</sup> and the orientationally averaged (isotropic) value of  $\gamma$  is evaluated, which is defined as

$$\langle \gamma \rangle = \frac{1}{15} \sum_{i,j} (\gamma_{ijj} + \gamma_{ijj} + \gamma_{iji}) \quad i, j = x, y, z \quad (2)$$

Taking the imaginary part of  $\langle \gamma \rangle$  value into the expression (1),  $\delta(\omega)$  can be acquired compared with the experimental data.

Thus, in this work, the molecular equilibrium geometries were carried out by the DFT method with CAM-B3LYP functional and 6-31G\* basis set. Then the time-dependent DFT (TD-DFT) method was applied to get the one-photon absorption spectra at the same level as stated before. Moreover, to better evaluate the one-photon absorption spectra, the properties of electronic excited states were also obtained by the ZINDO method to compare with these by TD-DFT. Furthermore, the two-photon absorption spectra, as well as the key physical parameters for the prediction of the two-photon absorption cross sections, were also performed by means of the ZINDO method, including the excitation energies and the transition moments. And then the second hyperpolarizability and the two-photon absorption cross sections were calculated by the FTRNLO-JLU program compiled by our group.

### 3. Results and discussion

#### 3.1 Molecular design and optimization method

So far, porphyrins have been a choice for NLO material area,<sup>36</sup> because of their macrocyclic structures offering easily modulated chemical, architectural flexibility, physical and optoelectronic features. On the other hand, the NLO properties of graphene have been explored by Wang *et al.*, showing broadband nonlinear optical response of graphene dispersions.<sup>37</sup> Therefore, considering that both graphene and porphyrin are potential NLO materials, the novel porphyrin-graphene hybrid materials may well possess better NLO properties. In an attempt to obtain some estimations of how the systematic change in molecular size and the introduction of porphyrin ultimately affect the OPA and TPA properties, particularly the TPA cross section values, we designed a series of molecules G<sub>n</sub> (n=1, 2, 3, 4, 5) and corresponding hybrid molecules TPP-NHCO-G<sub>n</sub> (n=1, 2, 3, 4, 5) based on graphene shown in Fig.1. In this work, pentacene is defined as the smallest in the sizes of the G<sub>n</sub> molecules, named G1, then expanding the molecular dimension to access G2, G3, G4, and G5, respectively. On the other hand, the structures of porphyrin-graphene hybrid materials have recently been experimentally studied,<sup>23</sup> demonstrating that there are several TPP (tetraphenyl porphyrin) covalently bonded together with graphene by –NHCO- bonds to improve the water solubility. However, considering the calculation condition as

well as the purpose to predict the properties of the hybrid materials using theoretical methods, each molecule of TPP-NHCO-Gn (n=1, 2, 3, 4, 5) possesses only one TPP in this work.

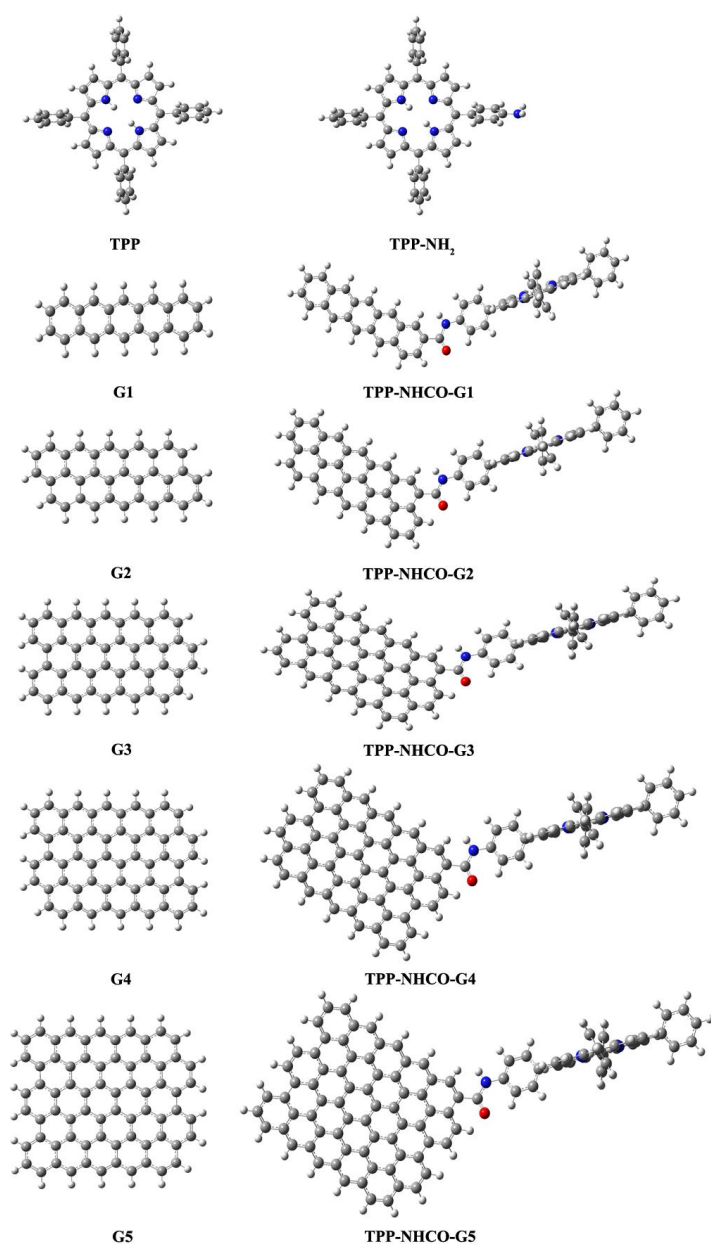


**Fig.1.** Optimized ground-state geometries of all studied molecules in this work.

From the optimized ground-state structures of TPP-NHCO-Gn, it is

found that when porphyrin is connected to Gn, the Gn moiety and the porphyrin fragment in hybrid molecules happen to be not in the same plane, there is a torsion angle between them as shown in Supporting Information, Fig.S1. It can be seen that the torsion angle in TPP-NHCO-G1 is the smallest ( $29^\circ$ ), but for TPP-NHCO-G2, it is  $44^\circ$ , then for TPP-NHCO-G3, TPP-NHCO-G4 and TPP-NHCO-G5, the torsion angles are the same, which is  $45^\circ$ , resulting from the effect of the steric hindrance. As a consequence, we hope the effort to modify the molecular structures by using a purely theoretical method can improve their photophysical properties and obtain some predictions of the structural modifications might affect their OPA and TPA features.

To get more accurate results by the TD-DFT method, the calculated results for G1 and TPP obtained by different functionals and the experimental data<sup>38,39,40</sup> are presented in Table 1. As clearly shown in Table 1, the calculated one-photon absorption and emission spectra of G1 molecule at TD-DFT//CAM-B3LYP/6-31G\* level are respectively 267.8 nm and 630.1 nm, which are in good agreement with the experimental values (273 nm and 639 nm).<sup>38</sup> In addition, the results of TPP are also in qualitative agreement with the experimental and theoretical data.<sup>39,40,41</sup> Moreover, no imaginary frequency is found for each optimized ground-state geometry of all molecules, verified by frequency calculations performed at DFT//CAM-B3LYP/6-31G\* level. Furthermore,

the CAM-B3LYP functional is usually considered to be well qualified to describe charge transfer character as mentioned in the theoretical methods section. Accordingly, the CAM-B3LYP functional with 6-31G\* basis set is appropriate for this target system.

**Table 1.** Calculated one-photon absorption and emission wavelengths as well as oscillator strengths ( $f$ ) for TPP and G1 with different TD-DFT methods and available experimental values

	TPP				G1			
	$\lambda_{max}^O/nm^a$	$f$	$\lambda_{ems}^O/nm^b$	$f$	$\lambda_{max}^O/nm^a$	$f$	$\lambda_{ems}^O/nm^b$	$f$
B3LYP/6-31G*	371.0	1.32	564.4	0.01	285.6	3.23	744.9	0.04
M06/6-31G*	372.6	1.48	596.2	0.03	285.9	3.29	736.2	0.05
<b>CAM-B3LYP/6-31G*</b>	<b>354.4</b>	<b>1.66</b>	<b>596.4</b>	<b>0.02</b>	<b>264.1</b>	<b>3.59</b>	<b>630.1</b>	<b>0.07</b>
PBE1PBE/6-31G*	365.6	1.43	576.5	0.04	280.5	3.35	719.6	0.04
Experimental data <sup>38,39,40</sup>	419 <sup>39,40</sup>		650 <sup>39,40</sup>		273 <sup>38</sup>		639 <sup>38</sup>	

<sup>a</sup>One-photon absorption spectra, <sup>b</sup>one-photon emission spectra.

### 3.2 Electronic structure

The frontier orbital energy levels (referred to four occupied orbitals, four unoccupied orbitals), and the energy gap values ( $\Delta E_{H-L}=E_{HOMO} - E_{LUMO}$ ) between the highest occupied molecular orbital (HOMO) and the lowest unoccupied molecular orbital (LUMO) of all studied molecules are analyzed, shown in Fig.2. Additionally, the molecular orbitals related to the main transitions of the OPA and TPA spectra (which are discussed in the next two sections) are also demonstrated in Fig.3 and Supporting Information, Fig.S2.

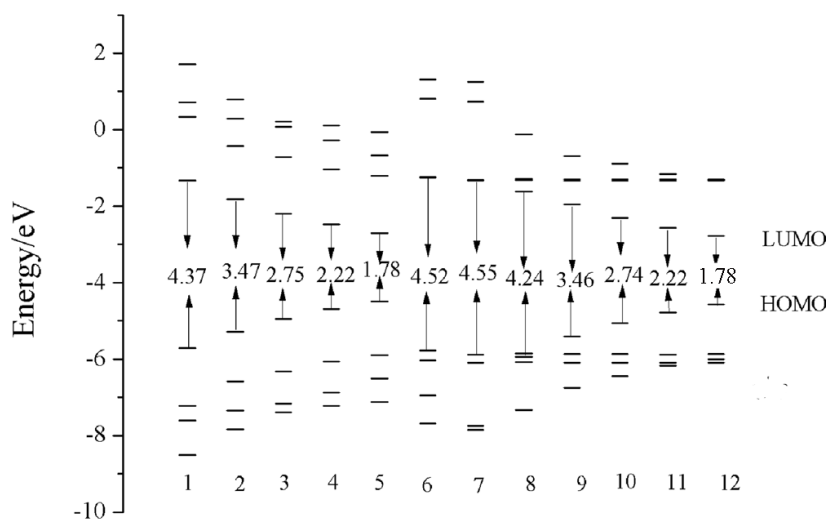


**Fig.2.** Frontier molecular orbital energies of molecules optimized at the DFT//CAM-B3LYP/6-31G\* level.

1–5 refer to G1→G5 molecules, 6 and 7 are respectively TPP and TPP-NH<sub>2</sub> molecules, and 8–12 represent TPP-NHCO-G1→TPP-NHCO-G5 molecules.

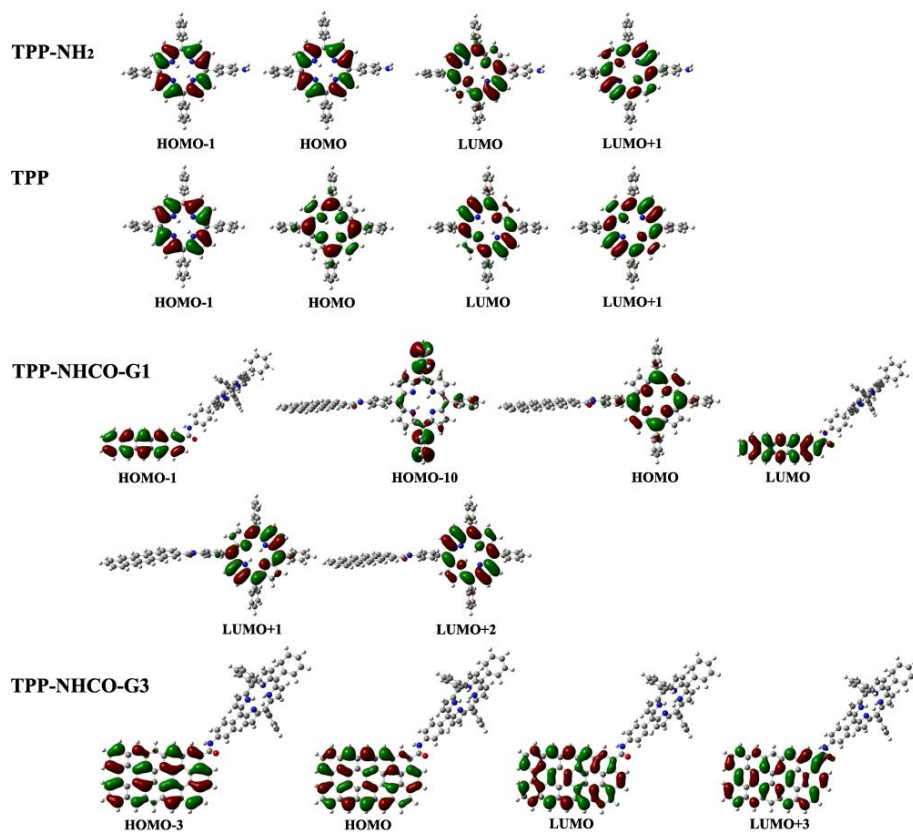


**Fig.3.** Some contour surfaces of the frontier molecular orbitals for the TPP, TPP-NH<sub>2</sub>,

TPP-NHCO-G1 and TPP-NHCO-G3 molecules.

Both TPP and TPP-NH<sub>2</sub> are tetrapyrrolic systems, they have common electronic structural properties, it is noted in Fig.2 that the LUMO and LUMO+1 orbitals in TPP-NH<sub>2</sub> and TPP are a set of quasi-degenerate orbitals, and the energy of the HOMO orbital is also approximate to that of the HOMO-1 orbital. Interestingly, they have two main absorption bands as shown in the spectra in Fig.4. Moreover, from the detailed values listed in Supporting Information Table S1 and Fig.3, it is found that these two main absorption bands are indeed caused by the transitions from the HOMO and HOMO-1 orbitals to the LUMO and LUMO+1 orbitals, which have a great influence on their TPA cross section values and are analyzed in the TPA discussion section.

In Fig.2, as the increase of n, the energy gap values gradually become lower and lower for both G<sub>n</sub> and hybrid molecules, attributing to the more enlargement of n, the more like graphene, whose energy gap is almost zero. Moreover, the decrease of the energy gap leads to the red-shifted absorption spectra. Compared to G<sub>n</sub>, the energy gap of the corresponding TPP-NHCO-G<sub>n</sub> is decreased, suggesting that the introduction of porphyrin has a significant impact on  $\Delta E_{H-L}$  and results in the red-shifted absorptions. On the other hand, both HOMO and LUMO are mainly constrained to the G<sub>n</sub> part of the hybrid molecules, except for the TPP-NHCO-G1 molecule, whose electron cloud in HOMO mainly

distributes on the porphyrin moiety, which probably because the size of G1 is much smaller than TPP, so the main electronic structural properties of TPP-NHCO-G1 more come from porphyrin, this profile can be illustrated from the main transition nature in Supporting Information, Fig.S2. From Table S1 and Fig.3, such as in the long wavelength range, both transitions from HOMO-2 to LUMO+1 and from HOMO-2 to LUMO+2 show the charge transfer from the porphyrin part to the porphyrin fragment, even though there is also interaction between the porphyrin moiety and the G1 fragment at other absorption peaks. What is more interesting, from Fig.2 and Fig.S2, is that the introduction of porphyrin actually provides some consistency of the degree of effects for TPP-NHCO-G<sub>n</sub> (n=1 – 5), whose the LUMO+1 and LUMO+2 orbitals are a set of quasi-degenerate orbitals, and whose the energy of LUMO+1 is almost the same, so does that of HOMO-1, HOMO-2 and LUMO+2. Overall, it looks like that the HOMO and LUMO orbitals of porphyrin are inserted between the HOMO and LUMO orbitals of separated G<sub>n</sub>. Retained orbitals such as LUMO+3 and HOMO-3 in TPP-NHCO-G<sub>n</sub> largely embody the profile of G<sub>n</sub>.

Meanwhile, as the increase of n, the energy levels from the G<sub>n</sub> part in TPP-NHCO-G<sub>n</sub> are denser, the  $E_{\text{LUMO}+3}$  value becomes lower and lower, which is more and more close to  $E_{\text{LUMO}+1}$  and  $E_{\text{LUMO}+2}$ . And for TPP-NHCO-G5, the energies of LUMO+3, LUMO+2 and LUMO+1 are

almost the same. Moreover, the  $E_{\text{HOMO-3}}$  of the hybrid molecules is gradually increasing, and the  $E_{\text{HOMO-2}}$  is almost the same among each hybrid molecule ( $n=1 - 4$ ) apart from TPP-NHCO-G5. In the case of TPP-NHCO-G5, the  $E_{\text{HOMO-3}}$  instead of its own  $E_{\text{HOMO-2}}$  approximates to  $E_{\text{HOMO-2}}$  of other hybrid molecules, as HOMO-1 is mainly constrained to the G5 fragment rather than the porphyrin moiety. It is notable that as the increase of  $n$ , the  $G_n$  part gradually dominates the main properties of TPP-NHCO- $G_n$ , especially TPP-NHCO-G4 and TPP-NHCO-G5, the  $\Delta E_{\text{H-L}}$  is barely affected by the introduction of porphyrin compared with the corresponding molecules G4 and G5, respectively. This implies that the size of the molecule ( $n=5$ ) is large enough to reflect the properties of the hybrid molecules well.

Therefore, as analyzed above, it is known that there is interaction between the  $G_n$  fragment and the porphyrin moiety in the novel hybrid molecules, who not only reserve the specialities of the two single fragments but also create excellent new features reflecting the interaction between the two parts. Thus, it is interesting to investigate if the size of  $G_n$  and the introduction of porphyrin both have a great influence on the electronic structures of the hybrid molecules, as well as the absorption properties and the TPA cross sections, which will be discussed in the next two sections 3.3 and 3.4.

### 3.3 One-photon absorption properties

On the basis of the optimized molecular structures, we perform TD-DFT//CAM-B3LYP/6-31G\* and ZINDO calculations to access the OPA spectra (UV-Vis spectra) for all molecules in this work. The OPA wavelengths ( $\lambda_{max}^O$ ), oscillator strengths ( $f$ ) and relevant transition characteristics of both methods are all collected in Supporting Information, Table S1, including available experimental data.

From Table S1, it can be concluded that the results obtained by the ZINDO method can commendably reflect the UV-Vis electronic spectra. Thus, in this study, we perform the calculations on the OPA and TPA properties of all studied molecules by the ZINDO method to figure out how the size of Gn and the introduction of the porphyrin, as well as the intramolecular charge transfer nature affect their properties, specifically TPA features.

To make the OPA spectra be more intuitive, the OPA spectra for all the studied molecules by ZINDO are presented in Fig.4. One can see that both TPP-NH<sub>2</sub> and TPP compounds have two dominant absorption regions, one at 300 – 400 nm and the other at 500 – 600 nm. These two regions of intense absorption are common for the porphyrin family and they are named as Soret- and Q-band, respectively. The transition features corresponding to the absorption bands are assigned and listed in Supporting Information Table S1, from which it can be observed that these two main bands are caused by the transitions from the HOMO and

HOMO-1 orbitals to the LUMO and LUMO+1 orbitals. In the porphyrin system, the Q-band is significant weaker in intensity than Soret-band because of the near-degeneracy of the LUMO and LUMO+1 orbitals in the free base macrocycle, which leads to a cancellation of the transition moments in the Q-region, and a complementary strengthening of the transition moments in the Soret-region.<sup>42</sup>

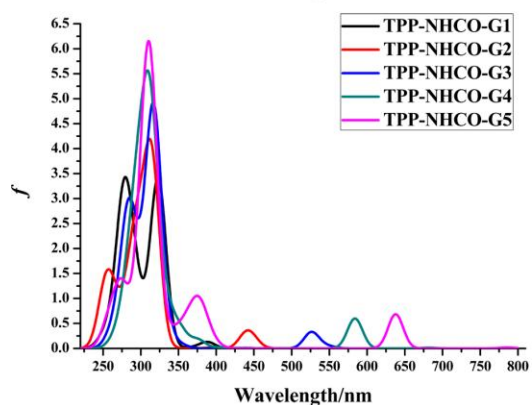
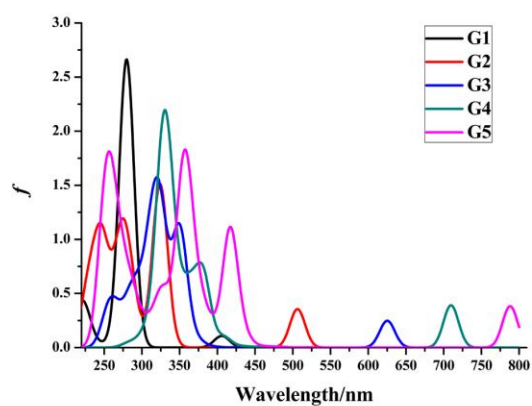
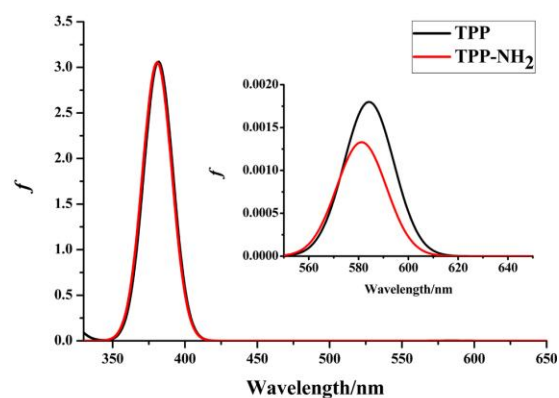


**Fig.4.** Simulated one-photon absorption spectra for the investigated molecules.

Moreover, from the absorption spectra of Gn, one can also see that the strongest absorption peak around 270 – 360 nm for all the Gn molecules exhibits red-shifts as the increase of n, that is, G1 (279.7 nm) < G2 (323.4 nm) < G3 (324.6nm) < G4 (328.2 nm) < G5 (359.2 nm). Surprisingly, except for G1 and G2, there occurs the second strong peak around 340 – 420 nm from G3 to G5, and G3 (350.1 nm) < G4 (380.9 nm) < G5 (416.8 nm). In addition, a small peak appears at 406.1 nm for G1, which corresponds to the small peaks of G2, G3, G4, and G5 at around 480 – 810 nm (can be seen from Fig.4), and this absorption peak of molecule G5 is about 382.0 nm red-shifted relative to that of molecule G1. More interestingly, adding each layer of pentacene makes the peak bathochromic-shifted by about 100 nm on average, such as G1 (406.1 nm), G2 (506.2 nm), G3 (625.2 nm), G4 (709.7 nm) and G5 (788.1 nm), and these absorption peaks for all molecules are assigned to  $\pi \rightarrow \pi^*$  character, arising from HOMO  $\rightarrow$  LUMO transition. Consequently, increasing the size of the molecules leads to a gradual bathochromic shift of the absorption band, which is just in accordance with the inference of the  $\Delta E_{H-L}$  aforementioned.

On the other hand, differing from Gn, the absorption peaks with the largest oscillator strengths are all focused around 310 – 320 nm for all the

hybrid molecules, but there are still small peaks around 370 – 800 nm. For TPP-NHCO-G1, the strongest peak covers a range of 320.2 – 326.1 nm, mainly resulting from the transitions of HOMO-10 → LUMO, HOMO-1 → LUMO, HOMO → LUMO+1, and HOMO → LUMO+2 (corresponding to 326.1 nm), and of HOMO-1 → LUMO, HOMO-1 → LUMO+2, and HOMO → LUMO (corresponding to 320.2 nm). From Fig.3, these transitions accompany the charge transfer from the porphyrin moiety to the G1 part, porphyrin to porphyrin fragment, and G1 to G1 moiety, respectively, indicating that there is strong interaction between the porphyrin part and the G1 moiety, and the respective electronic properties of G1 and porphyrin are retained. Besides, TPP-NHCO-G3 and TPP-NHCO-G5 have the same transition features at the strongest absorption, which suggests that the charge transfer exists in-between the single moieties (porphyrin or Gn), as well as the two fragments (porphyrin and Gn). On the contrary, for TPP-NHCO-G2 and TPP-NHCO-G4, there is only the charge transfer from the porphyrin part to the porphyrin moiety, from the G2 part to the G2 fragment, and from the G4 moiety to the G4 portion without charge transfer from the porphyrin fragment to the G2 or G4 segment at the strongest peak, which is probably ascribed to less symmetry of the Gn fragment in the even-number hybrid molecules than that in the odd-number hybrid molecules, and this feature requires further studies.

### 3.4 Two-photon absorption properties

In this section, based on the reasonable OPA results by the ZINDO approach, we performed calculations on the TPA physical parameters for all the molecules using the same method to estimate how the choice of changing the size ( subsection 3.4.1 ) and introducing porphyrin (subsection 3.4.2), as well as the internal factors of the TPA process (subsection 3.4.3) might affect the TPA properties, especially the TPA cross sections. According to expressions (1) and (2), the third-order polarizability  $\gamma(-\omega; \omega, -\omega, \omega)$  and the TPA cross sections are obtained through single and double electronic excitation configuration interaction (SDCI) by the ZINDO program, as well as FTRNLO-JLU compiled by our group. For all the molecules studied, the configuration interaction (CI)-active spaces are restricted to the 1682 singly excited configurations, and 425 doubly excited configurations.

The calculations on the TPA cross sections include the contributions of 300 lowest-lying excited states for each molecule. In order to ensure that the 300 excited states chosen are sufficient for the convergence of the TPA cross sections for all the studied molecules in this work, we took TPP-NHCO-G5 which is the biggest one among all the studied molecules as an illustration to obtain the description of the relationship between the third-order polarizability and the number of the excited states shown in Fig.5, revealing that when the chosen number of states reaches to 260, the

third-order polarizability has been already stable. Thus, we concluded that the 300 excited states are enough for the convergence of  $\delta_{max}$  for all the studied molecules.

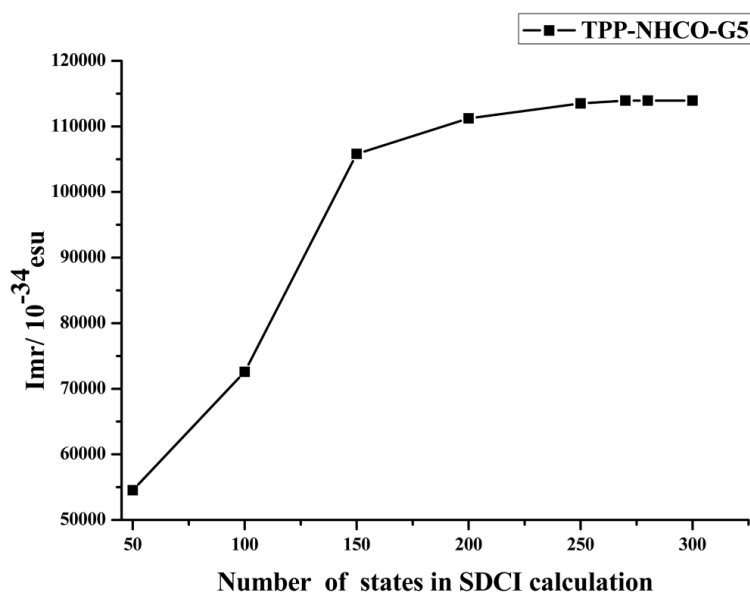


**Fig.5.** Relationship between the number of states and the third-order polarizability of TPP-NHCO-G5.

Moreover, in order to evaluate the accuracy of our calculated TPA cross sections, we firstly performed the calculation on the  $\delta_{max}$  value of TPP which has been experimentally researched, and the calculated  $\delta_{max}$  value is 98 GM, which is in reasonable agreement with the experimental results (730nm,  $35 \pm 20$  GM),<sup>39,40</sup> so we used the same parameters to calculate the  $\delta_{max}$  values of all the studied molecules by ZINDO. The detailed values, including TPA peaks ( $\lambda_{max}^T$ ), maximum TPA cross section ( $\delta_{max}$ ), and transition nature, are all listed in Table 2. Furthermore, the well-defined

TPA spectra are determined over a broad spectral range plotted in Fig.6.

**Table 2.** Calculated two-photon absorption properties of the studied molecules

Molecule	$\lambda_{max}^T/nm^a$	$\delta_{max}/GM^b$	Channel	Transition nature <sup>d</sup>	
TPP	749.6 730 <sup>c</sup>	98.0 35 ± 20 <sup>c</sup>	$S_0 \rightarrow S_8 \rightarrow S_9$	(HOMO-1,HOMO)→(LUMO,LUMO+1)	42.9%
				(HOMO-1,HOMO-1)→(LUMO+1,LUMO+1)	12.2%
				(HOMO,HOMO)→(LUMO,LUMO)	12.6%
				(HOMO,HOMO)→(LUMO+1,LUMO+1)	11.4%
				(HOMO-1,HOMO-1)→(LUMO,LUMO)	10.4%
TPP-NH <sub>2</sub>	746.9	101.8	$S_0 \rightarrow S_8 \rightarrow S_9$	(HOMO-1,HOMO-1)→(LUMO,LUMO)	10.2%
				(HOMO,HOMO)→(LUMO+2,LUMO+2)	14.2%
				(HOMO-1,HOMO)→(LUMO,LUMO+1)	41.0%
				(HOMO,HOMO)→(LUMO,LUMO)	12.1%
				(HOMO,HOMO)→(LUMO+1,LUMO+1)	10.8%
G1	550.1	67.9	$S_0 \rightarrow S_1 \rightarrow S_9$	(HOMO-2)→(LUMO)	51.3%
				(HOMO)→(LUMO+2)	38.7%
G2	694.2	148.6	$S_0 \rightarrow S_2 \rightarrow S_8$	(HOMO)→(LUMO+5)	20.0%
G3	814.6	176.7	$S_0 \rightarrow S_2 \rightarrow S_7$	(HOMO)→(LUMO+3)	17.0%
				(HOMO-1,HOMO)→(LUMO,LUMO+1)	12.1%
G4	876.8	913	$S_0 \rightarrow S_2 \rightarrow S_8$	(HOMO-2)→(LUMO)	10.9%
				(HOMO)→(LUMO+2)	26.3%
				(HOMO-1,HOMO)→(LUMO,LUMO+1)	14.2%
G5	926.6	1324.5	$S_0 \rightarrow S_2 \rightarrow S_7$	(HOMO-2)→(LUMO)	11.5%
				(HOMO)→(LUMO+2)	22.2%
				(HOMO)→(LUMO+3)	13.8%
TPP-NHCO-G1	680.5 500.7	114.6 739.6	$S_0 \rightarrow S_9 \rightarrow S_{19}$ $S_0 \rightarrow S_{20} \rightarrow S_{53}$	(HOMO-2)→(LUMO+3)	69.5%
				(HOMO-1)→(LUMO+14)	16.0%
TPP-NHCO-G2	615.6 520.9	269.6 1358.5	$S_0 \rightarrow S_7 \rightarrow S_{29}$ $S_0 \rightarrow S_7 \rightarrow S_{60}$	(HOMO-2)→(LUMO+4)	11.6%
				(HOMO)→(LUMO+5)	10.1%
				(HOMO)→(LUMO+7)	19.8%
				(HOMO-7)→(LUMO+4)	18.5%
				(HOMO,HOMO)→(LUMO,LUMO+4)	17.3%
TPP-NHCO-G3	873.2 569.9	62.8 3241.1	$S_0 \rightarrow S_2 \rightarrow S_{10}$ $S_0 \rightarrow S_2 \rightarrow S_{57}$	(HOMO-3)→(LUMO)	54.7%
				(HOMO)→(LUMO+3)	34.5%
TPP-NHCO-G4	772.0 636.5	1104.5 3738.8	$S_0 \rightarrow S_3 \rightarrow S_{17}$ $S_0 \rightarrow S_3 \rightarrow S_{44}$	(HOMO-5)→(LUMO+3)	14.9%
				(HOMO)→(LUMO+4)	32.3%
				(HOMO-8)→(LUMO)	20.3%
TPP-NHCO-G5	855.1	1416.1	$S_0 \rightarrow S_3 \rightarrow S_{13}$	(HOMO)→(LUMO+11)	13.0%
				(HOMO-4)→(LUMO)	11.0%
				(HOMO)→(LUMO+4)	29.1%
				(HOMO,HOMO)→(LUMO,LUMO)	11.4%

---

691.9	3904.3	S <sub>0</sub> →S <sub>3</sub> →S <sub>36</sub> (HOMO-3,HOMO)→(LUMO,LUMO+3)	17.4%
-------	--------	---	-------

---

<sup>a</sup>Calculated TPA spectra by the ZINDO program (see Theoretical methods); <sup>b</sup>TPA cross sections are given in GM (1 GM=1×10<sup>-50</sup> cm<sup>4</sup> · photon<sup>-1</sup>); <sup>c</sup>experimental data from ref. 39 and ref. 40; <sup>d</sup>dominant contributions and corresponding percentage of each electronic configuration forming an electron transition state.

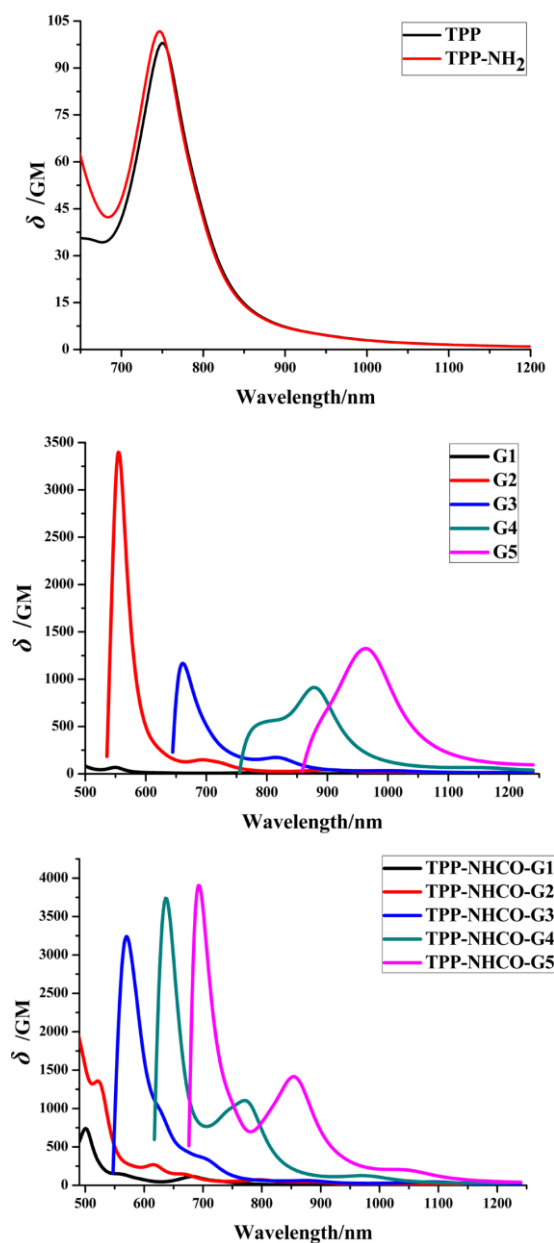


**Fig.6.** Two-photon absorption spectra for all of the studied molecules.

As observed from Fig.6 and Table 2, the  $\delta_{max}$  values of the G<sub>n</sub> molecules and some of the studied hybrid molecules display the intense

two-photon absorption in the NIR region with large TPA cross sections (1000 – 3900 GM), suggesting that these hybrid molecules can be novel promising molecules suitable for practical two-photon absorption materials. The later sections are devoted to discussing structural and some other aspects affecting the TPA properties. To avoid the interference from the OPA spectra, the TPA peaks in the spectral range of 500 – 1250 nm are discussed in the next subsections.

### 3.4.1 Size effect of molecule Gn

From Fig.6 and Table 2, it can be observed that as the increase of n, the  $\delta_{max}$  values of the Gn molecules significantly increase (67.9 GM  $\rightarrow$  148.6 GM  $\rightarrow$  176.7 GM  $\rightarrow$  913 GM  $\rightarrow$  1324.5 GM), and the  $\lambda_{max}^T$  value is marked bathochromic shift (550.1 nm  $\rightarrow$  694.2 nm  $\rightarrow$  814.6 nm  $\rightarrow$  876.8 nm  $\rightarrow$  926.6 nm), which demonstrates that the enlargement of the size leads to the significant increase of the  $\delta_{max}$  values because of the extended electron-delocalization, the same trends occur in TPP-NHCO-Gn, which is discussed in the next section in combination with the effect of the introduction of porphyrin.

### 3.4.2 Effect of the introduction of porphyrin

As shown in Fig.6 and Table 2, compared with Gn, the  $\delta_{max}$  values of TPP-NHCO-Gn (n=1, 2, 3, 4, 5) molecules distinctly enlarge with the increase of n in a range of 500 – 1250 nm of the TPA spectra, and all the hybrid molecules have two main TPA cross section peaks in this long

wavelength range. What is more, it is interesting to see that the TPA cross sections in the long-wavelength range for both TPP-NHCO-G1 and TPP-NHCO-G2 are 2-fold larger than that of corresponding G1 and G2. Furthermore, in the case of TPP-NHCO-G1, whose two-photon absorption at 680.5 nm mainly arises from the transition from HOMO-2 to LUMO+3, accompanying the charge transfer from the porphyrin part to the G1 moiety. For TPP-NHCO-G2, the TPA at 615.6 nm mainly comes from the transitions from HOMO-2 to LUMO+4, HOMO to LUMO+5, and HOMO to LUMO+7, and the corresponding charge transfer is from the porphyrin to G2 moiety, G2 to G2 fragment, and G2 to porphyrin part, respectively. Therefore, the charge transfer characters between the two parts are responsible for the enlargement of the TPA cross sections of TPP-NHCO-G1 and TPP-NHCO-G2.

Additionally, for the hybrid molecules, starting from TPP-NHCO-G3, the TPA cross sections in the long-wavelength range barely increase compared with the corresponding Gn molecules shown in Table 2, that is, TPP-NHCO-G3 (62.8 GM), TPP-NHCO-G4 (1104.5 GM) and TPP-NHCO-G5 (1416.1 GM) compared with G3 (176.7 GM), G4 (913 GM) and G5 (1324.5 GM), respectively, which is probably because that the charge transfer only occurs from Gn (n=3, 4, 5) to Gn (n=3, 4, 5) part without the interaction between the porphyrin part and the Gn (n=3, 4, 5) segment. Taking TPP-NHCO-G3 for instance, its two-photon absorption

is mainly the transitions assigned from HOMO-3 to LUMO and HOMO to LUMO+3. Combining Fig.3, one can see that the charge transfer is just from the G3 to G3 fragment, and the similar case also occurs in TPP-NHCO-G4 and TPP-NHCO-G5. Consequently, we concluded that such a two-photon absorption peak in the three hybrid molecules largely exhibits the properties of G3, G4, and G5.

Further, it is important to emphasize that porphyrin has a vital role on the larger TPA cross sections of the hybrid molecules. With the introduction of porphyrin, the larger TPA cross sections in the short-wavelength range substantially increase, that is, TPP-NHCO-G1 (739.6 GM) < TPP-NHCO-G2 (1358.5 GM) < TPP-NHCO-G3 (3241.1 GM) < TPP-NHCO-G5 (3904.3 GM), which are much larger than these of the corresponding G<sub>n</sub> molecules. For example, the  $\delta_{max}$  value of the TPP-NHCO-G3 molecule (3241.1 GM) is 18 times greater than that of G3 (176.7 GM), and its two-photon absorption is mainly caused by the transition from HOMO-5 to LUMO+3, the relevant charge transfer is from the benzene ring of the porphyrin fragment to the G3 moiety, implying that the interaction between the two parts contributes significantly to the enlargement of the  $\delta_{max}$  value. Likewise, this feature also arises in other hybrid molecules, especially TPP-NHCO-G4 and TPP-NHCO-G5, whose the interaction between the two parts is more obvious than that in TPP-NHCO-G3, as the charge transfer is from the

porphyrin core to the Gn (n=4, 5) part. For TPP-NHCO-G4, its TPA transition mainly comes from HOMO-8 to LUMO, along with the charge transfer from the porphyrin core to the G4 part, and the same trend occurs in TPP-NHCO-G5 whose the excitations are associated with the charge transfer corresponding predominantly to the transitions from the HOMO-3 and HOMO orbitals to the LUMO and LUMO+3 orbitals shown in Table 3. Furthermore, HOMO-3 and HOMO are respectively constrained to the porphyrin part and the G5 fragment, while LUMO and LUMO+3 are respectively located to the G5 moiety and the porphyrin fragment (see Supporting Information, Fig.S2), revealing that a stronger interaction appears in the TPP-NHCO-G5 molecule, what makes its  $\delta_{max}$  value larger than that of the TPP-NHCO-G3 and TPP-NHCO-G4 molecules.

In one word, as discussed above, the introduction of porphyrin enhancing the intramolecular charge transfer is responsible for the distinct increase of the TPA cross sections to a large extent.

### 3.4.3 Influence of molecular chemical structure

This subsection is focused on the internal factors that affect the two-photon absorption process and the TPA properties.

Generally, the position and relative strength of the two-photon resonance can be predicted by the following three-level energy model simplified form of the SOS expression:<sup>34,35,43</sup>

$$\delta \propto \frac{M_{0k}^2 M_{kn}^2}{(E_{0k} - E_{0n} / 2)^2 \Gamma} + \frac{M_{0n}^2 \Delta\mu_{0n}^2}{(E_{0n} / 2)^2 \Gamma} \quad (3)$$

Here,  $M_{\alpha\beta}$  and  $E_{\alpha\beta}$  are respectively the transition dipole moment and the corresponding excitation energy from the state  $\alpha$  to  $\beta$ ; the subscripts 0,  $k$ , and  $n$  respectively refer to the ground state  $S_0$ , the intermediate state  $S_k$ , and the two-photon absorption final state  $S_n$ ;  $\Delta\mu_{0n}$  is the state dipole moment difference between ground state  $S_0$  and final state  $S_n$ ; the damping factor  $\Gamma$  was set to 0.14 eV. As shown in Supporting Information, Fig.S3, it is confirmed that  $\delta_{max}$  is roughly proportional to  $X$  ( $X = \frac{M_{0k}^2 M_{kn}^2}{(E_{0k} - E_{0n} / 2)^2 \Gamma} + \frac{M_{0n}^2 \Delta\mu_{0n}^2}{(E_{0n} / 2)^2 \Gamma}$ ), that is, the position and relative strength of the two-photon resonance in this system can be predicted according to the three-level energy model. In this context, some important physical parameters of the two-photon absorption of the studied compounds are listed in Table 3. Moreover, to more intuitively observe which factor has a greater impact on the  $\delta_{max}$  values, the relationships of  $\delta_{max}$  versus the factors are drawn in Supporting Information, Fig.S4.

**Table 3.** Calculated important parameters of two-photon absorption of the studied molecules

	$M_{0k}$ /Debye	$M_{kn}$ /Debye	$M_{0n}$ /Debye	$E_{0k}-E_{0n}/2$ /eV	$E_{0n}/2$ /eV	$\Delta\mu_{0n}$ /Debye	$\text{Im}\gamma$ / $10^{-34}$ esu	$\delta_{max}$ /GM	$X$
TPP	11.4	2.77	0.00	1.61	1.65	0.00	3339.0	98.0	2747.8
TPP-NH <sub>2</sub>	11.0	2.75	2.00	1.62	1.66	0.31	3442.3	101.8	2491.5
G1	3.02	2.55	0.00	0.59	2.47	0.001	1245.8	67.9	1237.8
G2	6.18	5.12	0.012	0.66	1.79	0.02	4340.3	148.6	16417.3
G3	5.78	5.47	0.24	0.48	1.51	0.15	6974.9	176.7	30989.9
G4	7.68	8.56	0.00	0.35	1.40	0.001	42557.0	913.0	252003.1
G5	8.01	8.61	0.64	0.30	1.27	0.28	74407.2	1324.5	377486.1

TPP-NHCO-G1	3.19	11.0	2.30	1.30	1.89	0.27	3216.0	114.6	5218.2
	10.3	2.46	1.64	1.36	2.45	10.3	11243.0	739.6	2813.2
TPP-NHCO-G2	5.13	6.20	1.21	0.81	2.01	2.43	6193.5	269.6	11041.5
	5.23	7.01	2.23	0.45	2.37	-0.12	22350.7	1358.5	45631.8
TPP-NHCO-G3	2.27	3.73	0.83	0.86	1.40	0.26	2900.5	62.8	696.1
	2.27	5.32	6.33	0.067	4.39	0.21	63752.7	3241.1	239143.8
TPP-NHCO-G4	8.61	9.53	0.62	0.53	1.59	-1.05	91823.5	1104.5	171204.6
	8.61	3.97	2.97	0.18	1.95	-0.69	91823.5	3738.8	267699.8
TPP-NHCO-G5	9.63	10.57	0.38	0.50	1.45	0.89	113311.1	1416.1	296029.6
	9.63	6.17	1.71	0.13	1.81	0.55	113311.1	3904.3	1471907

Furthermore, it can be seen from Table 3 that as the enlargement of the size of the Gn molecules, the values of  $M_{kn}$  (the transition dipole moment between the intermediate state and final state) are enhanced, as well as  $M_{0k}$  (the transition dipole moment between the ground state and intermediate state). In addition, the introduction of porphyrin induces a slight decrease in the detuning term ( $E_{0k} - E_{0n}/2$ ) value and the enhancement of  $M_{0k}$  and  $M_{kn}$  compared with that of the corresponding Gn molecules, which can be observed from Fig.S4 in Supporting Information, except for the TPP-NHCO-G3 molecule, which has the smallest energy tuning term value resulting in the sharp increase of  $\delta_{max}$  (3241.1 GM). Moreover, the introduction of porphyrin makes the  $M_{0k}$  and  $M_{kn}$  values of the hybrid molecules closer and closer as the increase of n, and the closer of the  $M_{0k}$  and  $M_{kn}$  values are, the greater of the  $\delta_{max}$  values are. Furthermore, the imaginary part of the third-order polarizability ( $Im\gamma$ ) increases as the enlargement of n, and the  $Im\gamma$  of TPP-NHCO-G5 reaches to the largest, thus, the largest  $\delta_{max}$  value.

As discussed above, it can be concluded that both the increase of the transition moments ( $M_{0k}$  and  $M_{kn}$ ) and the decrease in the energy tuning term ( $E_{0k} - E_{0n}/2$ ), resulting from the introduction of porphyrin and the increasing size of the molecules, play a crucial role in determining the TPA cross sections. By the analysis of Table 3 and Fig.S4 in Supporting Information, the substitution of porphyrin changes the  $M_{0k}$  and  $M_{kn}$  values, thus, the  $\delta_{max}$  values of the hybrid molecules become larger and larger as the increase of  $n$ , since the  $M_{0k}$  values become more and more close to the  $M_{kn}$  values. We believe that the variance of the transition dipole moments contributes importantly to the changing trends of the  $\delta_{max}$  values for the TPP-NHCO-Gn molecules.

#### 4. Conclusion

In this work, we firstly designed a series of novel molecules Gn ( $n=1, 2, 3, 4, 5$ ) based on graphene and the corresponding porphyrin-Gn hybrid molecules named TPP-NHCO-Gn ( $n=1, 2, 3, 4, 5$ ), then predicted their one-photon absorption (OPA) and two-photon absorption (TPA) characteristics by employing the TD-DFT and ZINDO methods combined with the FTRNLO-JLU program compiled by our group. The calculated results demonstrate that the ultraviolet absorption spectra of the Gn molecules are in a range of 300 – 400 nm, and the TPA cross sections ( $\delta_{max}$ ) visibly increase (67.9 – 1324.5 GM) as the enlargement of the size occurring in the wavelengths ranging from 550.1 to 926.6 nm. In addition,

the introduction of porphyrin avails the hybrid molecules to possess better nonlinear optical properties and solubility, as well as much higher TPA cross sections attributing to the intramolecular charge transfer between the porphyrin moiety and the Gn fragment compared to these of the corresponding Gn molecules, especially the TPP-NHCO-G3, TPP-NHCO-G4 and TPP-NHCO-G5 molecules, which have considerable TPA cross sections, that is, 3241.1, 3738.8 and 3904.3 GM, respectively. Thus, the hybrid molecules are more attractive to be applied as the two-photon absorption materials in optical limiting and two-photon fluorescence microscopy (TPFM) fields. Besides, to make it clear how the molecular size and the introduction of porphyrin affect the TPA process, the approximate sum-over-states (SOS) expression is used to analyze the intrinsic reasons for the changing trends of the TPA cross sections of the investigated molecules. It suggests that the introduction of porphyrin results in the  $M_{0k}$  values (the transition dipole moment between the ground state and intermediate state) of the TPP-NHCO-Gn (n=1 – 5) molecules becoming more and more close to these of the  $M_{kn}$  values (the transition dipole moment between the intermediate state and final state) as the gradual increase of n accompanying apparently enlargement of the TPA cross sections, revealing that the increase of the transition dipole moments is the dominant factor of the enlargement of the  $\delta_{max}$  values. Moreover, it is also found that the hybrid molecules not only display the

respective properties of porphyrin and Gn, but also show their distinctive characteristics because of the interaction between the two parts. Overall, we forecast that the TPA features of the porphyrin-Gn (TPP-NHCO-Gn) hybrid molecules are better than graphene-like (Gn). We expect this study can provide some theoretical basis for the synthesis of the novel TPA materials based on graphene for further applications.

### Acknowledgements

This work is supported by the Natural Science Foundation of China (Nos. 21173099, 20973078 and 20673045), the Major State Basis Research Development Program (2013CB 834801) and special funding to basic scientific research projects for Central Colleges.

### Supporting Information

OPA properties of the studied molecule calculated by the time-dependent DFT method and ZINDO method, contour surfaces of the frontier orbitals relevant to the OPA and TPA processes, the relationships of  $\log\delta_{max}$  and  $\log X$ , and the relationships between  $\delta_{max}$  and the impact factors.

### References and notes

1. (a) C. N. LaFratta, J. T. Fourkas, T. Baldacchini and R. A. Farrer, *Angew. Chem., Int. Ed.*, 2007, **46**, 6238-6258; (b) T. F. Scott, B. A. Kowalski, A. C. Sullivan, C. N. Bowman and R. R. McLeod, *Science*, 2009, **324**, 913-917.
2. M. G. Silly, L. Porrès, O. Mongin, P. A. Chollet and M. B. Desce, *Chem. Phys.*

- Lett.*, 2003, **379**, 74-80.
3. M. Velusamy, J. Y. Shen, J. T. Lin, Y. C. Lin, C. C. Hsieh, C. H. Lai, C. W. Lai, M. L. Ho, Y. C. Chen, P. T. Chou and J. K. Hsiao, *Adv. Funct. Mater.*, 2009, **19**, 2388-2397.
  4. J. J. Jasieniak, I. Fortunati, S. Gardin, R. Signorini, R. Bozio, A. Martucci and P. Mulvaney, *Adv. Mater.*, 2008, **20**, 69-73.
  5. X. J. Feng, P. L. Wu, F. Bolze, H. W. Leung, K. F. Li, N. K. Mak, D. W. Kwong, J. F. Nicoud, K. W. Cheah and M. S. Wong, *Org. Lett.*, 2010, **12**, 2194-2197.
  6. K. S. Novoselov, A. K. Geim, S. V. Morozov, D. Jiang, Y. Zhang, S. V. Dubonos, I. V. Grigorieva and A. A. Firsov, *Science*, 2004, **306**, 666-669.
  7. D. Li and R. B. Kaner, *Science*, 2008, **320**, 1170-1171.
  8. D. A. Dikin, S. Stankovich, E. J. Zimney, R. D. Piner, G. H. Dommett, G. Evmenenko, S. T. Nguyen and R. S. Ruoff, *Nature*, 2007, **448**, 457-460.
  9. J. S. Bunch, A. M. van der Zande, S. S. Verbridge, I. W. Frank, D. M. Tanenbaum, J. M. Parpia, H. G. Craighead and P. L. McEuen, *Science*, 2007, **315**, 490-493.
  10. A. K. Geim and K. S. Novoselov, *Nat. Mater.*, 2007, **6**, 183-191.
  11. G. Eda, G. Fanchini and M. Chhowalla, *Nat. Nanotechnol.*, 2008, **3**, 270-274.
  12. H. A. Becerril, J. Mao, Z. F. Liu, R. M. Stoltenberg, Z. A. Bao and Y. S. Chen, *ACS Nano*, 2008, **2**, 463-470.
  13. Z. F. Liu, Q. Liu, Y. Huang, Y. F. Ma, S. G. Yin, X. Y. Zhang, W. Sun and Y. S.

- Chen, *Adv. Mater.*, 2008, **20**, 3924-3930.
14. X. Wang, L. J. Zhi and K. Müllen, *Nano Lett.*, 2008, **8**, 323–327.
15. (a) Z. S. Wu, W. Ren, L. Wen, L. Gao, J. P. Zhao, Z. P. Chen, G. G. Zhou, F. Li and H. M. Cheng, *ACS Nano*, 2010, **4**, 3187–3194.
- (b) D. H. Wang, R. Kou, D. W. Choi, Z. G. Yang, Z. M. Nie, J. Li, L. V. Saraf, D. H. Hu, J. G. Zhang, G. L. Graff, J. Liu, M. A. Pope and I. A. Aksay, *ACS Nano*, 2010, **4**, 1587–1595.
16. (a) J. Pyun, *Angew. Chem., Int. Ed.*, 2011, **50**, 46–48.
- (b) A. R. Siamaki, A. E. R. S. Khder, V. Abdelsayed, M. S. El-Shall and B. F. Gupton, *J. Catal.*, 2011, **279**, 1–11.
17. S. Niyogi, E. Bekyarova, M. E. Itkis, J. L. McWilliams, M. A. Hamon and R. C. Haddon, *J. Am. Chem. Soc.*, 2006, **128**, 7720-7721.
18. Y. X. Xu, H. Bai, G. Lu, C. Li and G. Q. Shi, *J. Am. Chem. Soc.*, 2008, **130**, 5856-5857.
19. S. Stankovich, D. A. Dikin, G. H. Dommett, K. M. Kohlhaas, E. J. Zimney, E. A. Stach, R. D. Piner, S. T. Nguyen and R. S. Ruoff, *Nature*, 2006, **442**, 282-286.
20. S. Stankovich, R. D. Piner, S. T. Nguyen and R. S. Ruoff, *Carbon*, 2006, **44**, 3342-3347.
21. Y. Si and E. T. Samulski, *Nano Lett.*, 2008, **8**, 1679-1682.
22. Y. F. Xu, Z. B. Liu, X. L. Zhang, Y. Wang, J. G. Tian, Y. Huang, Y. F. Ma, X. Y. Zhang and Y. S. Chen, *Adv. Mater.*, 2009, **21**, 1275-1279.

23. M. B. Krishna, V. P. Kumar, N. Venkatramaiah, R. Venkatesan and D. N. Rao, *Appl. Phys. Lett.*, 2011, **98**, 081106.
24. M. J. Frisch, G. W. Trucks, H. B. Schlegel, G. E. Scuseria, M. A. Robb, J. R. Cheeseman, G. Scalmani, V. Barone, B. Mennucci, G. A. Petersson, H. Nakatsuji, M. Caricato, X. Li, H. P. Hratchian, A. F. Izmaylov, J. Bloino, G. Zheng, J. L. Sonnenberg, M. Hada, M. Ehara, K. Toyota, R. Fukuda, J. Hasegawa, M. Ishida, T. Nakajima, Y. Honda, O. Kitao, H. Nakai, T. Vreven, J. A. Montgomery, J. E. Peralta, F. Ogliaro, M. Bearpark, J. J. Heyd, E. Brothers, K. N. Kudin, V. N. Staroverov, R. Kobayashi, J. Normand, K. Raghavachari, A. Rendell, J. C. Burant, S. S. Iyengar, J. Tomasi, M. Cossi, N. Rega, J. M. Millam, M. Klene, J. E. Knox, J. B. Cross, V. Bakken, C. Adamo, J. Jaramillo, R. Gomperts, R. E. Stratmann, O. Yazyev, A. J. Austin, R. Cammi, C. Pomelli, J. W. Ochterski, R. L. Martin, K. Morokuma, V. G. Zakrzewski, G. A. Voth, P. Salvador, J. J. Dannenberg, S. Dapprich, A. D. Daniels, Farkas, J. B. Foresman, J. V. Ortiz, J. Cioslowski and D. J. Fox, *Gaussian 09*, Revision B.01; *Gaussian Inc.: Wallingford, CT*, 2010.
25. A. D. Becke, *J. Chem Phys.*, 1993, **98**, 5648.
26. T. Yanai, D. P. Tew and N. C. Handy, *Chem. Phys. Lett.*, 2004, **393**, 51-57.
27. M. J. Peach, T. Helgaker, P. Salek, T. W. Keal, O. B. Lutnaes, D. J. Tozer and N. C. Handy, *Phys. Chem. Chem. Phys.*, 2006, **8**, 558-562.
28. M. C. Zerner, J. E. Ridley, A. D. Bacon, W. D. Edwards, J. D. Head, J. McKelvey, J. C. Culberson, P. Knappe, M. G. Cory, B. Weiner, J. D. Baker,

- W. A. Parkinson, D. Kannis, J. Yu, N. Roesch, M. Kotzian, T. Tamm, M. M. Karelson, X. Zheng, G. Pearl, A. Broo, K. Albert, J. M. Cullen, C. J. Cramer, D. G. Truhlar, J. Li, G. D. Hawkins and D. A. Liotard, ZINDO 99.1.
29. M. Cha, W. E. Torruellas, G. I. Stegeman, W. H. G. Horsthuis, G. R. Möhlmann and J. Meth, *Appl. Phys. Lett.*, 1994, **65**, 2648-2650.
30. T. Kogej, D. Beljonne, F. Meyers, J. W. Perry, S. R. Marder, and J. L. Brédas, *Chem. Phys. Lett.*, 1998, **298**, 1-6.
31. B. J. Orr and J. F. Ward, *Mol. Phys.*, 1971, **20**, 513-526.
32. D. M. Bishop, J. M. Luis and B. Kirtman, *J. Chem Phys.*, 2002, **116**, 9729.
33. Y. Zhao, A. M. Ren, J. K. Feng and C. C. Sun, *J. Chem Phys.*, 2008, **129**, 014301.
34. D. Beljonne, W. Wenseleers, E. Zojer, Z. Shuai, H. Vogel, S. J. K. Pond, J. W. Perry, S. R. Marder and J. L. Brédas, *Adv. Funct. Mater.*, 2002, **12**, 631-641.
35. M. Albota, D. Beljonne, J. L. Brédas, J. E. Ehrlich, J. Y. Fu, A. A. Heikal, S. E. Hess, T. Kogej, M. D. Levin, S. R. Marder, D. McCord-Maughon, J. W. Perry, H. Röckel, M. Rumi, G. Subramaniam, W. W. Webb, X. L. Wu and C. Xu, *Science*, 1998, **281**, 1653-1656.
36. M. O. Senge, M. Fazekas, E. G. A. Notaras, W. J. Blau, M. Zawadzka, O. B. Locos and E. M. Ni Mhuirheartaigh, *Adv. Mater.*, 2007, **19**, 2737-2774.
37. J. Wang, Y. Hernandez, M. Lotya, J. N. Coleman and W. J. Blau, *Adv. Mater.*, 2009, **21**, 2430-2435.
38. Y. Wang, P. Wu, C. X. Xu and Y. P. Cui, *Chin. J. Electron Dev.*, 2005, **28**,

- 269-270.
39. M. Kruk, A. Karotki, M. Drobizhev, V. Kuzmitsky, V. Gael and A. Rebane, *J. Lumin.*, 2003, **105**, 45-55.
40. X. Z. Yan, T. Goodson, T. Imaoka and K. Yamamoto, *J. Phys. Chem. B*, 2005, **109**, 9321-9329.
41. J. Arnbjerg, A. J. Banzo, M. J. Paterson, S. Nonell, J. I. Borrell, O. Christiansen and P. R. Ogilby, *J. Am. Chem. Soc.*, 2007, **129**, 5188-5199.
42. L. T. Bergendahl and M. J. Paterson, *J. Phys. Chem. B*, 2012, **116**, 11818-11828.
43. M. Rumi, J. E. Ehrlich, A. A. Heikal, J. W. Perry, S. Barlow, Z. Y. Hu, D. M. Maughon, T. C. Parker, H. Röckel, S. Thayumanavan, S. R. Marder, D. Beljonne and J. L. Brédas, *J. Am. Chem. Soc.*, 2000, **122**, 9500-9510.

**Graphical abstract:****Theoretical investigations on one- and two-photon absorptions for a series of covalently functionalized hybrid materials based on graphene**

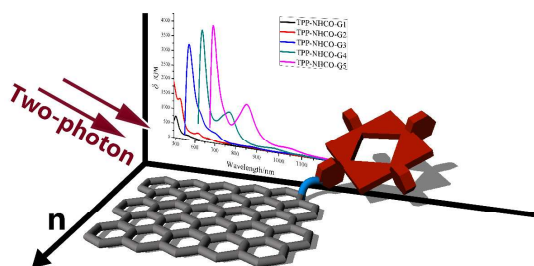
Li Zhang,<sup>1</sup> Lu-Yi Zou,<sup>1</sup> Jing-Fu Guo,<sup>2</sup> Ai-Min Ren\*,<sup>1</sup> Dan Wang,<sup>1</sup> Ji-Kang Feng<sup>1</sup>

<sup>1</sup>State Key Laboratory of Theoretical and Computational Chemistry,  
Institute of Theoretical Chemistry, Jilin University,  
Changchun 130061, People's Republic of China

<sup>2</sup>School of Physics, Northeast Normal University, 130024, P. R. China

\*Corresponding author: Tel./fax: +86-431-88498567 (A. M. Ren)

E-mail addresses: aimin\_ren@yahoo.com



Graphene-based (Gn) hybrids with porphyrin possess improved solubility and good nonlinear optical properties, especially excellent two-photon absorption (TPA) features.